

A SEARCH FOR FALLBACK DISKS IN FOUR YOUNG SUPERNOVA REMNANTS

ZHONGXIANG WANG, DAVID L. KAPLAN^{1,2}, AND DEEPTO CHAKRABARTY²

Kavli Institute for Astrophysics and Space Research, Massachusetts Institute of Technology, Cambridge, MA 02139

Draft version May 20, 2018

ABSTRACT

We report on our search for the optical/infrared counterparts to the central compact objects in four young supernova remnants: Pup A, PKS 1209–52, RCW 103, and Cas A. The X-ray point sources in these supernova remnants are excellent targets for probing the existence of supernova fallback disks, since irradiation of a disk by a central X-ray source should lead to an infrared excess. We used ground-based optical and near-infrared imaging and *Spitzer Space Telescope* mid-infrared imaging to search for optical/infrared counterparts at the X-ray point source positions measured by the *Chandra X-Ray Observatory*. We did not detect any counterparts, and hence find no evidence for fallback disks around any of these sources. In PKS 1209–52, we are able to exclude a nearby optical/infrared candidate counterpart. In RCW 103, a blend of 3 faint stars at the X-ray source position prevents us from deriving useful limits. For the other targets, the upper limits on the infrared/X-ray flux ratio are as deep as $(1.0\text{--}1.7)\times 10^{-4}$. Comparing these limits to the ratio of $\approx 6 \times 10^{-5}$ measured for 4U 0142+61 (a young pulsar recently found with an X-ray irradiated dust disk), we conclude that the non-detection of any disks around young neutron stars studied here are consistent with their relatively low X-ray luminosities, although we note that a similar dust disk around the neutron star in Pup A should be detectable by deeper infrared observations.

Subject headings: ISM: individual (Puppis A, PKS 1209–52, RCW 103, Cassiopeia A) — supernova remnants — X-rays: stars — stars: neutron

1. INTRODUCTION

Neutron stars (NSs) are formed when massive stars end their lives during core-collapse supernovae. During such an explosion, “fallback” may occur when the reverse shock, caused by the impact of the shock wave with the outer stellar envelope, reaches the newly formed NS (Chevalier 1989; Woosley & Weaver 1995). Depending upon the rotation rate of the massive progenitor, some of the fallback may have sufficient angular momentum to form a disk (Michel & Dessler 1981; Lin, Woosley, & Bodenheimer 1991). Although widely predicted by contemporary numerical studies of supernovae (Woosley & Weaver 1995), there are few observational constraints on the existence of fallback disks or even of supernova fallback generally. Fallback could have profound implications for the endgame of massive star evolution, particularly since it could lead a newborn NS to collapse into a black hole (Chevalier 1989). Such an outcome might yet explain the lack of a detectable pulsar in SN 1987A (Zampieri et al. 1998; Fryer, Colgate, & Pinto 1999). Supernova fallback is also a promising mechanism for producing the debris disks necessary to form planets (Phinney & Hansen 1993; Podsiadlowski 1993), which are known to exist around at least one pulsar (Wolszczan & Frail 1992; Wolszczan 1994).

The compact stellar remnants of supernovae obviously probe supernova physics. While it was once thought that young radio pulsars like those in the Crab and Vela supernova remnants (SNRs) were prototypical of newborn

NSs, it has recently been realized that the young NS population is unexpectedly diverse. For example, there are a few young SNRs currently known to contain radio-quiet, non-plerionic X-ray point sources near their geometric center (see Pavlov, Sanwal, & Teter 2004, hereafter PST04, for a review). These X-ray point sources, often called central compact objects (CCOs), have X-ray spectra roughly consistent with the thermal-like surface (but smaller than the expected neutron star surface) emission from young cooling NSs. However, they differ from “typical” young NSs (e.g., the Crab pulsar) in SNRs in that they lack strong non-thermal emission components and most of them do not have detectable pulsations. Along with other young NS classes including the anomalous X-ray pulsars (AXPs), and soft gamma-ray repeaters (Woods & Thompson 2004), these objects challenge our standard framework for understanding young NSs.

Because CCOs and AXPs do not have the strong, broad-band, non-thermal emission typically observed from young Crab-like pulsars and their associated synchrotron nebulae, they offer an attractive opportunity for testing the existence of fallback disks by detecting their expected thermal emission. Perna, Hernquist, & Narayan (2000) showed that the combination of an untruncated outer edge of a fallback disk (in contrast to a binary accretion disk) and irradiation of the disk by the central pulsar should lead to a strong thermal excess in the infrared and submillimeter bands. In a previous paper, we reported the detection of a mid-infrared counterpart to the AXP 4U 0142+61, which we interpreted as dust emission from an X-ray heated debris disk around the pulsar (Wang, Chakrabarty, & Kaplan 2006). Here, we report our ground-based optical/near-IR and *Spitzer Space Telescope* 4.5/8.0 μm observations of four CCOs. These

Electronic address: wangzx, dlk, deepto@space.mit.edu

¹ Pappalardo Fellow

² Also Department of Physics, Massachusetts Institute of Technology, Cambridge, MA 02139

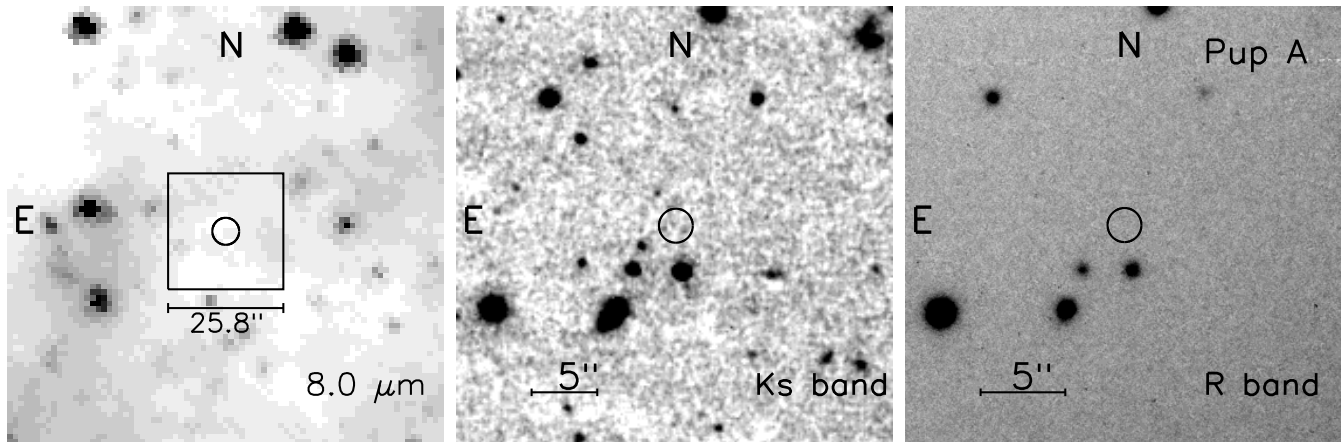


FIG. 1.— Optical and IR images of RX J0822.0–4300. The *Chandra* error circle (solid circle) of the CCO is indicated in the optical *R* (right panel) and near-IR *K_s* (middle panel) bands images. The left panel shows the *Spitzer*/IRAC 8.0 μm band image, with the box and circle indicating the size of the *R* and *K_s* images and the CCO position respectively. The circle is not to scale. No object was found within the error circle.

targets were selected from a total of 8 known CCOs because they are relatively young and their distances are well determined (PST04). We give brief summaries of our targets in § 1.1. We then present the optical/IR observations in § 2. Finally, we present our results in § 3 and our conclusions in § 4. Part of our ground-based observations have previously been reported (Wang & Chakrabarty 2002).

1.1. Target Summary

Of the four CCOs that we observed, the basic properties of these sources are similar: young, radio quiet, and X-ray bright, with roughly similar X-ray spectra (again, see PST04). However, some have distinguishing characteristics, as we note below. We also describe observations of their host SNRs used to determine ages and distances, fundamental quantities that we use in the interpretation of the observations. A summary of the general properties of the CCOs that we observed is given in Table 1.

RX J0822.0–4300 (Pup A) The X-ray source RX J0822.0–4300 (Petre et al. 1982; Petre, Becker, & Winkler 1996) is located in the SNR Puppis A (Pup A; G260.4–3.4). The SNR is the remnant of a Type II explosion that occurred < 5000 yrs ago (Winkler et al. 1988; Arendt, Dwek, & Petre 1991). The distance to the SNR, determined from associated H I absorption, is 2.2 ± 0.3 kpc (Reynoso et al. 2003). The CCO is unremarkable, except that Hui & Becker (2005) recently reported a possible detection of 0.22-s X-ray pulsations.

1E 1207.4–5209 (PKS 1209–52) The source 1E 1207.4–5209 (Helfand & Becker 1984) is in the SNR PKS 1209–52 (G296.5+10.0). This SNR has a distance of $2.1^{+1.8}_{-0.8}$ kpc based on associated H I gas (Giacani et al. 2000) and an age of ≈ 7 kyr (Roger et al. 1988). The CCO is the only confirmed pulsator among the sources considered here ($P_{\text{spin}}=424$ ms; Zavlin et al. 2000;

Pavlov et al. 2002c) although its spin does not change monotonically (Zavlin, Pavlov, & Sanwal 2004), and its X-ray spectrum is quite unique with a number of related X-ray absorption features (Sanwal et al. 2002; Bignami et al. 2003).

1E 161348–5055.1 (RCW 103) The CCO 1E 161348–5055.1 (Tuohy & Garmire 1980) is in the SNR RCW 103 (G332.4–0.4). The distance to the SNR of 3.1 kpc has been estimated from an H I association (Reynoso et al. 2004), while the age of ≈ 2 kyr was determined from measurement of the expansion of optical filaments (Carter, Dickel, & Bomans 1997). Unlike the other objects, the CCO has shown considerable X-ray variability on a timescale of years (Gotthelf, Petre, & Vasisht 1999; Becker & Aschenbach 2002), and at least three faint near-infrared sources have been found within the $0''.7$ *Chandra* X-ray position uncertainty (PST04). Together, these facts suggest that 1E 161348–5055.1 is a low-mass X-ray binary with a 6.4 hr orbital period (Becker & Aschenbach 2002; PST04).

CXOU J232327.8+584842 (Cas A)

CXOU J232327.8+584842 (Tananbaum 1999) is in the SNR Cassiopeia A (Cas A; G111.7-2.1), the youngest known Galactic core-collapse SNR (≈ 300 yr; Thorstensen, Fesen, & van den Bergh 2001), but the CCO was only revealed recently (compared to the others, which had been identified by the *Einstein Observatory*) by the *Chandra* X-ray Observatory (Tananbaum 1999; Pavlov et al. 2000; Chakrabarty et al. 2001). Comparing proper motions and radial velocities of ejecta, Reed et al. (1995) estimate a distance of $3.4^{+0.3}_{-0.1}$ kpc. The X-ray properties are, like those of RX J0822.0–4300, unremarkable, and this CCO serves as a benchmark for the class. Deep optical/near-IR observations of the source field

were conducted (Kaplan, Kulkarni, & Murray 2001; Fesen, Pavlov, & Sanwal 2006), but no counterpart was found.

2. OBSERVATIONS

2.1. Ground-based Observations

We obtained ground-based observations of the three southern targets among our sample of four CCOs. A summary of these observations is given in Table 2. Below we briefly list the observations, and discuss the reduction and calibration procedures.

We obtained optical images of the fields around the CCOs RX J0822.0–4300, 1E 1207.4–5209, and 1E 161348–5055.1 using the Magellan Instant Camera (MagIC) at an f/11 Nasmyth focus of both the 6.5 m Baade (Magellan I) and Clay (Magellan II) telescopes (Shectman & Johns 2003) at Las Campanas Observatory in Chile. MagIC is a 2048×2048 SiTe CCD with a 0′′.069 pixel^{−1} plate scale and a 142′′ field of view. We observed the standard stars SA 107–614 and Ru 152 (Landolt 1992; Smith et al. 2002) to calibrate the Baade data, while for the Clay data we also observed a number of Stetson³ standard fields with both MagIC and the Las Campanas 40-inch telescope. We reduced the MagIC data using the IRAF data analysis package, first subtracting bias images and then applying flat-fields.

We obtained JHK_s near-IR images of the RX J0822.0–4300 and 1E 1207.4–5209 fields using the Ohio State Infrared Imager/Spectrometer (OSIRIS; Depoy et al. 1993) at the f/14 tip-tilt focus of the 4 m Blanco Telescope at the Cerro Tololo Inter-American Observatory (CTIO) in Chile. The detector in OSIRIS was a Rockwell HAWAII HgCdTe 1024×1024 array. We used the OSIRIS f/7 camera, which had a 0′′.161 pixel^{−1} plate scale and a 93′′ field of view. During each exposure, we dithered the telescope in a 3×3 grid with offsets of about 10′′ to allow for correction of the rapidly variable infrared sky background and to minimize the effect of bad pixels. The near-IR standard stars SJ 9136 (HST S165-E) and SJ 9157 (HST S273-E) were observed for flux calibration (Persson et al. 1998).

We then obtained JHK_s images of our target fields with the “ClassicCam” near-infrared imager (Persson et al. 1992) at an f/11 Nasmyth focus on the Baade Telescope. The detector was a Rockwell NICMOS3 HgCdTe 256×256 array. We operated the camera in its low-resolution mode, with a 0′′.112 pixel^{−1} plate scale and a 29′′ field of view. The same dithering and data reduction was employed as with the CTIO observations. The near-IR standard star SJ 9172 (HST S279-F) was observed (Persson et al. 1998).

Finally, we obtained deep near-IR images of the 1E 1207.4–5209 field under excellent conditions using the Baade telescope and Persson’s Auxiliary Nasmyth Infrared Camera (PANIC; Martini et al. 2004), which contains a Rockwell 1024×1024 detector with a 0.125′′ plate scale. The telescope position was dithered five times with a 15′′ dither step, over the course of each exposure. The standard star SJ 9172 was also observed.

As with the optical data, the IRAF data analysis package was used for the data reduction, including bias sub-

traction and flat fielding. From each set of the dithered near-IR images, a sky image was derived by filtering out stars. The sky image was then subtracted from the set of images, and a final target field image was obtained by average combining the sky-subtracted images.

We astrometrically calibrated all of our ground-based optical and near-IR images by matching unsaturated field stars to USNO-A2.0 astrometric catalog stars (Monet 1998). We used 24, 46, and 50 stars in calibrating RX J0822.0–4300, 1E 1207.4–5209, and 1E 161348–5055.1 respectively. We used the IRAF task `ccmap` to derive the astrometric solutions. The uncertainties in matching the stars are negligible. The nominal uncertainties of the calibrated images are dominated by the USNO-A2.0 catalog systematic uncertainty ($\simeq 0′′.25$; Monet 1998).

2.2. Spitzer/IRAC Mid-IR Observations

We observed the four CCOs with the *Spitzer Space Telescope* using the Infrared Array Camera (IRAC; Fazio et al. 2004), an imaging camera operating at wavelengths of 3.6, 4.5, 5.8, and 8.0 μm . One pair of the detectors of the IRAC, either 3.6/5.8 μm or 4.5/8.0 μm , observes one field of view simultaneously: we used the 4.5/8.0 μm detectors. The detectors at the short and long wavelengths are InSb and Si:As devices respectively, with 256×256 pixels and a plate scale of 1′′.2, giving a field of view of 5′.2×5′.2. The frame time we used was 100 s, with 96.8 s effective exposure time per frame for the 4.5 μm data and 93.6 s effective exposure time for the 8.0 μm data.

The data were processed through the data reduction pipelines (version S11.0; IRAC Data Handbook 2004) at the *Spitzer* Science Center. In the basic calibrated data (BCD) pipeline, the individual flux-calibrated frames were produced from the raw images. The BCD frames were then average combined into the post-BCD (PBCD) mosaics. In the PBCD pipeline, each frame was astrometrically calibrated with respect to the detected Two Micron All-Sky Survey (2MASS; Skrutskie et al. 2006) stars, resulting in a position accuracy⁴ of $< 0′′.3$.

Our IRAC observations did not detect any mid-IR counterparts to the CCOs. The sensitivity of IRAC observations is dominated by a combination of background sky emission and confusion, with the latter dominating when a field is crowded. We measured the IRAC sky brightnesses at our target positions (§ 2.3), and we give those values in Table 3. As can be seen, Pup A and PKS 1209-52 have low background emission while Cas A has medium/high background emission⁵, caused somewhat by diffuse emission from the SNR; the high background of RCW 103 is presumably caused by its crowded field. To determine upper limits to the presences of point sources in the IRAC images, we converted the PBCD images of our targets in units of MJy/sr to data numbers (DN), and derived the 3σ upper limits (given in Table 4) from the standard deviation of the background sky at the source positions.

2.3. X-ray Positions

⁴ See <http://www.ipac.caltech.edu/2mass/releases/allsky/doc/explsup.h>

⁵ See <http://www.spitzer.caltech.edu/obs/bg.html> for a dis-

³ <http://cadwww.dao.nrc.ca/cadcbn/wdbi.cgi/astrocat/stetson/quesion> of *Spitzer* background levels

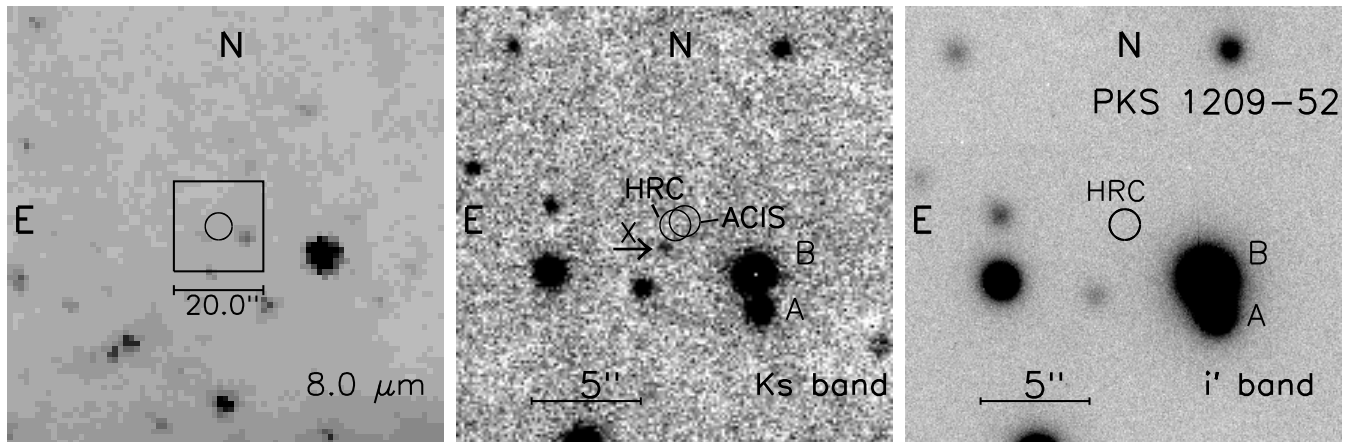


FIG. 2.— Optical/IR images of the 1E 1207.4–5209 region. In the left panel, the *Spitzer*/IRAC 8.0 μm band image is shown, with the box and circle indicating the size of the middle and right panel images and the CCO position respectively. The circle is not to scale. In the middle panel, a K_s band image is shown. The two solid circles indicate the *Chandra* HRC and ACIS positions, which are about $1''.0$ away from the object labeled X . The right panel shows the optical i' band image of the target field. The near-IR object was not detected by our optical observations, but was found with $V \simeq 26.8$ by Pavlov et al. (private communication). Previous observations have identified the two blended stars (A and B) as main sequence stars (Matsui, Long, & Tuohy 1988; Bignami, Caraveo, & Mereghetti 1992; see also De Luca et al. 2004).

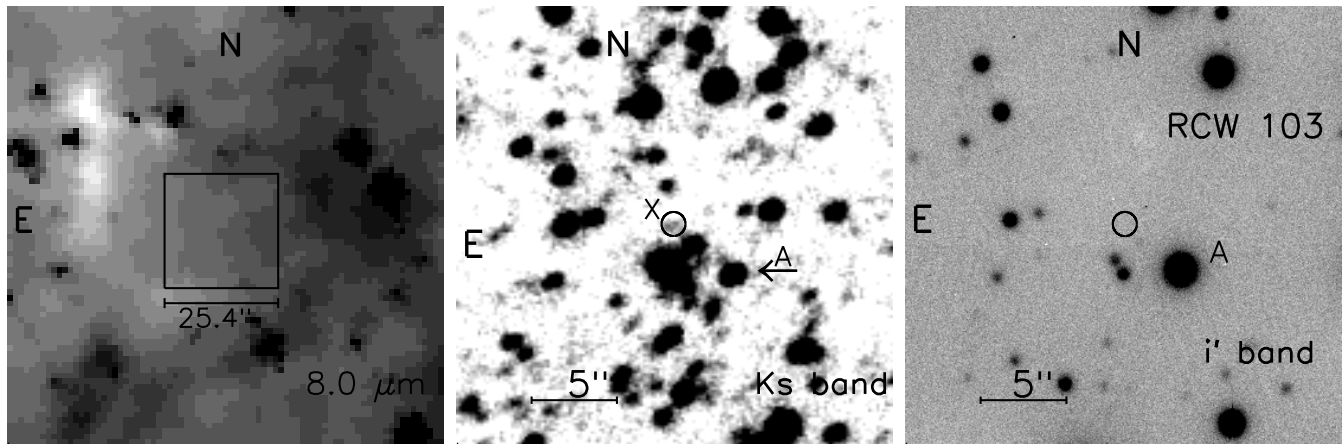


FIG. 3.— Optical/IR images of the region around 1E 161348–5055.1. The left panel shows the *Spitzer*/IRAC 8.0 μm band image of the field with the box indicating the size of the K_s and i' images, shown in the middle and right panel respectively. The CCO position is at the center of the box, and no object was found. One object, probably consisting three faint objects as reported by PST04, was detected by the near-IR observations within the $0''.7$ *Chandra* error circle (middle panel). The object was not detected by our optical observations, as indicated by the right panel image. Object A was identified as a subdwarf M star by Tuohy et al. (1983).

The X-ray positions of the CCOs reported in the literature were not of the uniformly high quality necessary for comparison with ground-based data. Where possible we took positions from published *Chandra X-Ray Observatory* results, but for three of the four sources we derived new positions from one or more observations retrieved from the *Chandra* public data archive. Using the CIAO thread `fix_offset`, we checked the data for any known aspect offsets and applied the corrections if necessary. The CIAO tool `wavdetect` was used for obtaining the source positions. We give all of the positions in Table 1, and discuss the observations of each source in more detail below. The total nominal position uncertainty for locating the CCOs on our optical/IR images is dominated by the *Chandra* absolute astrometric uncertainty

($\approx 0''.6$ with a 90% confidence). To estimate the effects of relative systematic astrometric errors between the optical/IR and *Chandra* images, we adopted the approach outlined in § 3.2.

3. RESULTS

3.1. *RX J0822.0–4300 (Pup A)*

For *RX J0822.0–4300* there are three *Chandra* observations made with the HRC-I (Obs_ID=749, exposure-time=18 ks), ACIS-S (Obs_ID=750, exposure-time=12 ks), and HRC-S (Obs_ID=1851, exposure-time=20 ks). The source positions we derived from the data generally differ by $0''.2$, consistent with the *Chandra* pointing uncertainty ($\approx 0''.6$ with a 90% confidence). We adopted the

position from ACIS-S data: R.A. = $08^{\text{h}}21^{\text{m}}57^{\text{s}}.42$ and Dec. = $-43^{\circ}00'16''.62$ (equinox J2000.0); ACIS-S positions have been tested more and should be more reliable (Fesen et al. 2006). The total nominal uncertainty of the position on the optical/near-IR images is $0''.7$ (90% confidence), dominated by the *Chandra* and USNO-A2.0 catalog systematic uncertainties. In Figure 1 we plot optical, near-, and mid-IR images of RX J0822.0–4300 and indicate the X-ray position as a solid circle in the middle and right panels of the figure. No objects were found near the position of RX J0822.0–4300, so we determined the 3σ limiting magnitudes from our observations and give them in Table 4.

3.2. 1E 1207.4–5209 (PKS 1209–52)

The source 1E 1207.4–5209 was observed with *Chandra*/ACIS several times between 2000 and 2003, but only the 2003 June 6 observation (Obs_ID=3913, exposure-time=20 ks) with ACIS-S was not under continuous clocking (CC) mode (which only allows derivation of one-dimensional source positions). From this observation we derive a position of R.A. = $12^{\text{h}}10^{\text{m}}00^{\text{s}}.92$ and Dec. = $-52^{\circ}26'28''.35$ (equinox J2000.0). In addition, there is an HRC-I observation made on 2003 December 28 (Obs_ID=4593, exposure time=50 ks) which gives the position R.A. = $12^{\text{h}}10^{\text{m}}00^{\text{s}}.88$ and Dec. = $-52^{\circ}26'28''.66$ (equinox J2000.0), differing by about $0''.5$ from the ACIS position, with the uncertainty on each of about $0''.7$ (90% confidence). In Figure 2, we indicate both ACIS and HRC positions; while the ACIS position should be more reliable (see above), since there is a source near the error circle of this CCO (see below) we show both positions to demonstrate that neither of them is consistent with the source.

As shown by the K_s image in Figure 2, we detected one faint object (labeled *X*) in our J and K_s near-IR images. We used the IRAF aperture photometry package APPHOT to measure the brightness of this object, finding $J = 22.2 \pm 0.3$ and $K_s = 21.1 \pm 0.2$. The detection of this object was also reported by PST04 ($V \simeq 26.8$, $K_s \simeq 20.7$), and it was suggested as a low mass dwarf (G. Pavlov, private communication). This object is the closest to the X-ray error circle, but is $1''.06$ away from the HRC position and $1''.36$ away from the ACIS position: both offsets are close to the positional uncertainty limit, with deviations of $\approx 3\sigma$ from the ACIS position and $\approx 2.5\sigma$ from the HRC position. Our further examination of the ACIS image found three X-ray sources coincident with stars from the USNO-A2.0 catalog. These stars, having 7–200 X-ray counts, were all within $3'$ of the ACIS aimpoint such that the astrometry should be of the highest quality⁶. The X-ray positions that we measured for the three stars differ by an average of $0''.11 \pm 0''.08$ in R.A. and $0''.34 \pm 0''.08$ in Dec. from the USNO positions, indicating that we would expect at most a $0''.7$ offset between X-ray and USNO positions (at 3σ confidence), which means that the $> 1''$ offset between *X* and 1E 1207.4–5209 is highly unlikely. As an independent check, our photometry indicates that the object is likely to be a background main-sequence star (M5 dwarf at a distance of 8 kpc). We therefore dismiss this source as an unrelated star. Aside from this object, we detect no

likely counterpart to the CCO, and so we give 3σ limiting magnitudes in Table 4.

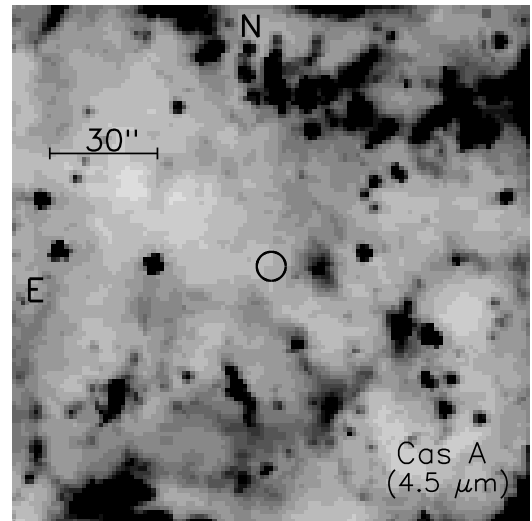


FIG. 4.— *Spitzer*/IRAC 4.5 μm band image of Cas A. The CCO position is indicated by a $4''.0$ radius circle (this is far larger than the position uncertainty, and is intended for ease of viewing). No counterpart was found.

3.3. 1E 161348–5055.1 (RCW 103)

The CCO 1E 161348–5055.1 has been monitored over the last few years with *Chandra*/ACIS, and most of the observations were short with 3.5–5 ks exposures. We analyzed the data taken on 1999 September 26 (Obs_ID=123, exposure-time=14 ks), and obtained the following position of 1E 161348–5055.1: R.A. = $16^{\text{h}}17^{\text{m}}36^{\text{s}}.25$ and Dec. = $-51^{\circ}02'24''.5$ (equinox J2000.0), which is consistent with that reported by Garmire et al. (2000). In Figures 3, we show the source position on our i' and K_s images of the field of 1E 161348–5055.1. For 1E 161348–5055.1, the total nominal uncertainty (90% confidence) on the optical/IR images, taking into account the *Chandra* pointing and USNO-A2.0 calibration uncertainties, is $0''.7$.

One object (labeled *X* in the middle panel of Figure 3) was detected at the *Chandra* position in our near-IR HK_s images. We used the IRAF photometry package DAOPHOT to measure the magnitudes of the stars in this crowded field, and found $H = 19.4 \pm 0.2$ and $K_s = 18.1 \pm 0.1$, along with a 3σ limiting magnitude of $J \geq 21.9$. We believe that this object is the same as one reported by Pavlov et al. (2002a), who measured $J \simeq 22.3$. PST04 subsequently used high-resolution ground-based and *Hubble Space Telescope* imaging to identify three faint late-type stars within the $0''.7$ *Chandra* error circle. Our object *X* probably corresponds to the blend of these. PST04 have suggested that 1E 161348–5055.1 may be an X-ray binary with a late-type companion. In bands other than H and K_s , we do not detect any counterpart, and hence give 3σ limiting magnitudes in Table 4. The limits are not as deep as those of the previous two sources because of higher background in this field.

⁶ Again, see <http://cxc.harvard.edu/cal/ASPECT/celmon/>.

3.4. CXOU J232327.8+584842 (Cas A)

We adopted the position given by Fesen et al. (2006) for CXOU J232327.8+584842, which is R.A. = $23^{\text{h}}23^{\text{m}}27^{\text{s}}.94$, Dec. = $+58^{\circ}48'42''.51$ (equinox J2000.0), with a 1σ uncertainty of $0''.4$. This position is indicated in Figure 4, where we display the $4.5\ \mu\text{m}$ IRAC image of the field. No mid-IR counterpart was detected in our data, so we give 3σ limiting magnitudes in Table 4. The limits are considerably less constraining than those of RX J0822.0–4300 because of the high background from the SNR.

4. DISCUSSION AND CONCLUSIONS

Based on the current observed properties, it is likely that the CCOs represent elements of a new class of young NSs, or even of several new classes (given their heterogeneous properties). Their overall characteristics — radio-quietness, distinct thermal X-ray emission, relatively long spin periods (when detected) for their ages, and lack of pulsar wind nebulae — indicate that they distinctively differ from other classes of young NSs, especially the young rotation-powered pulsars. The possible origin of the CCOs has been well discussed by comparing them to different types of NS objects and models, which include the rotation-powered pulsars, AXPs, magnetars, accreting binaries, accreting NSs from a residual disk (e.g., Chakrabarty et al. 2001; PST04; Gotthelf et al. 2005). Among them, one intriguing model is that the CCOs are NSs accreting from a residual disk, probably formed from fallback of supernova material. This model was primarily proposed as an alternative to the magnetar model for AXPs in order to explain their “anomalous” natures: that their X-ray luminosities are much higher than their rotational energy loss rates (e.g., Chatterjee, Hernquist, & Narayan 2000; Marsden et al. 2001). However, the X-ray fluxes of most of the CCOs, especially our targets (e.g., Zavlin et al. 2004; Fesen et al. 2006), have been steady based on the observations over the past few years, contrary to the fact that accreting X-ray sources are highly variable (this is in contrast to 1E 161348–5055.1, which PST04 therefore exclude from the CCO category). In addition, the optical observations of CCOs have failed to detect any counterparts that could be an accretion disk (e.g., Fesen et al. 2006; Gotthelf et al. 2005). Particularly for 1E 1207.4–5209, which is the least reddened among the CCOs, the optical observations (including ours) were deep enough to exclude the existence of an accretion disk around it (except an edge-on disk, which has very low probability; Zavlin et al. 2004). Therefore, even though the CCOs are probably not a uniform class of objects, it is very unlikely that their X-ray emission is powered by accretion.

However, it is still possible that isolated, young NSs have cool, passive disks. Such a disk would be farther away from a central NS and cooler than an accretion disk. If they exist, the disks would not contribute to generating X-ray emission from young NSs such as the CCOs and AXPs, but their existence might help explain various phenomena of radio pulsars (Michel & Dessler 1981; Blackman & Perna 2004; Cordes & Shannon 2006), planets formation around NSs (Lin et al. 1991), or the diversity of young NSs (Alpar

2001). The recent discovery of the mid-IR emission from the AXP 4U 0142+61 probably indicates the existence of such a passive disk around that young pulsar (Wang et al. 2006). The disk, irradiated by the X-rays from the central X-ray pulsar, emits mainly in the IR (Figure 5). Using *Spitzer*/IRAC observations similar to those discussed here, its unabsorbed IR-to-X-ray flux ratio was found to have a maximum value of $(\nu_{4.5\mu} F_{4.5\mu})/F_X \simeq 6.3 \times 10^{-5}$ at $4.5\ \mu\text{m}$. This ratio, as it depends largely on the geometry of the disk and not on the peculiarities of the central object, might be typical for any dust disks around young NSs. In Figure 5, we compare the upper limits on the IR/X-ray flux ratios of the CCOs to the same ratios of 4U 0142+61. The upper limits on the IR/X-ray flux ratios of the CCOs are not sufficiently deep to detect a disk similar to that found in 4U 0142+61. As the X-ray luminosities of the CCOs are typically lower ($\simeq 2 \times 10^{33}\ \text{erg s}^{-1}$; see Table 1), deeper IR exposures are needed in order to reach a comparable IR/X-ray flux ratio. Accordingly, in order to further explore any existence of dust disks around the CCOs, RX J0822.0–4300 would be a plausible target. For example, a $4.5\ \mu\text{m}$ flux of $0.6\ \mu\text{Jy}$ would be expected from a dust disk, which is detectable by deep *Spitzer*/IRAC observations (several hours exposure time). In comparison, for the very young CCO CXOU J232327.8+584842, although mid-IR observations are less affected by reddening ($A_V \simeq 7$; Fesen et al. 2006), diffuse emission of the SNR highly contaminates the source field, making it extremely difficult to have a sensitive search.

It is interesting to compare the flux ratio limits to those of the Crab-like, rotation-powered pulsars, even though it is clear that their optical/IR emission is non-thermal, originating from the magnetospheres of the pulsars. For several well-studied rotation-powered pulsars, optical/IR emission can be connected to nonthermal hard X-rays with a same power-law (e.g., PSR B0656+14; Pavlov, Zavlin, & Sanwal 2002b). The connection may be further indicated by a similar optical to nonthermal-X-ray flux ratio, $F_{\text{opt}}/F_X^{\text{nonth}} \simeq 0.001\text{--}0.01$, where F_{opt} is the optical flux between $4000\text{--}9000\ \text{\AA}$ and F_X^{nonth} is the non-thermal X-ray flux between $1\text{--}10\ \text{keV}$ (Zavlin & Pavlov 2004). In Figure 5, we also show the unabsorbed SED of the Crab pulsar, normalized by its X-ray flux ($1.5 \times 10^{36}\ \text{ergs s}^{-1}$; Zavlin & Pavlov 2004). The SED is above most of the upper limits on the CCOs, indicating that our observations would have detected Crab-like young pulsars. This comparison has additionally shown that the CCOs are a different class of young NSs from the typical Crab-like pulsars.

Our optical/IR observations have additionally provided strong constraints on the binary model proposed for the CCOs. As the upper limits of our observations of RX J0822.0–4300 and 1E 1207.4–5209 are 24–26 mag in the optical and 20–23 mag in the near-IR (or $\nu F_\nu \leq 5 \times 10^{-15}\ \text{erg s}^{-1}\ \text{cm}^{-2}$; see Figure 5 and note that the X-ray fluxes are around $10^{-12}\ \text{erg s}^{-1}\ \text{cm}^{-2}$), they would have detected main-sequence stars down to spectral type M5 regardless of extinction or white dwarfs down to effective temperature $T_{\text{eff}} \simeq 10^4\ \text{K}$ (Bergeron, Wesemael, & Beauchamp 1995), assuming relatively low extinction (e.g., $A_V \leq 1\text{--}2$; Predehl & Schmitt 1995; see Table 1), out to distances

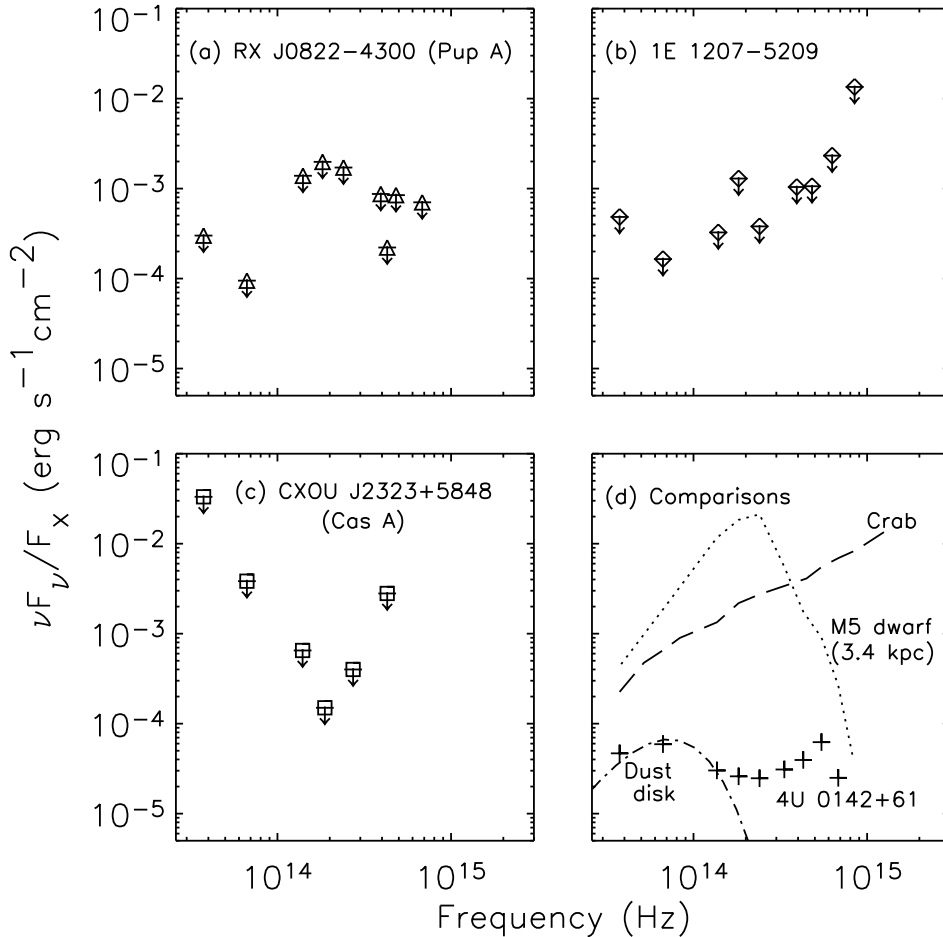


FIG. 5.— Upper limits on the optical/IR to X-ray flux ratio for the CCOs: (a) RX J0822.0–4300 ; (b) 1E 1207.4–5209 ; (c) CXOU J232327.8+584842 (the optical/near-IR *RJHK* upper limits are from Fesen et al. 2006). Fluxes are unabsorbed, and $A_V = 1.6, 0.5,$ and 7 are respectively used for dereddening the optical/IR data (according to the reddening laws of Schlegel, Finkbeiner, & Davis 1998 for the *BVR*I data, Fan 1999 for the *u'g'r'i'* data, Rieke & Lebofsky 1985 for the *JHK* data, and Indebetouw et al. 2005 for the IRAC data). (d) Optical/IR to X-ray flux ratios (for comparison) of the AXP 4U 0142+61 (plus sign; Wang et al. 2006) and the Crab pulsar (long-dashed curve; Eikenberry et al. 1997; Temim et al. 2006, in preparation). The IR component of 4U 0142+61 is likely to be due to an X-ray irradiated dust disk (dash-dotted curve). The optical/IR observations should also have detected a main-sequence star down to M5 (dotted curve; from Cox 2000 and Kurucz 1993, and normalized to a typical 0.4–8.0 keV CCO X-ray flux 2×10^{-12} erg cm $^{-2}$ s $^{-1}$) even at a distance of 3.4 kpc.

of 2–3 kpc.

In summary, we have obtained deep multi-wavelength observations of four CCOs in young SNRs. The observations have allowed us to find a near-IR counterpart to the CCO in RCW 103, which probably corresponds to three faint late type stars resolved by high-resolution observations. In addition, the observations have detected a low mass star close to, but inconsistent with, the current *Chandra* positions of 1E 1207.4–5209. The non-detection of any IR emission from debris disks around three of the CCOs could be due to their relatively low X-ray luminosities, compared to 4U 0142+61. While high background prohibits additional observations of two of the sources, deeper IR observations of RX J0822.0–4300 could probe the existence of a fallback disk around this CCO.

IRAF is distributed by the National Optical Astronomy Observatories, which are operated by the Association of Universities for Research in Astronomy, Inc., under cooperative agreement with the National Science Foundation. The Digitized Sky Surveys were produced at the Space Telescope Science Institute under U.S. Government grant NAG W-2166. This research has made use of the data products from the Two Micron All Sky Survey, which is a joint project of the University of Massachusetts and the Infrared Processing and Analysis Center/Caltech, funded by NASA and NSF.

Facilities: Spitzer (IRAC), Magellan:Baade (ClassicCam, MagIC, PANIC), Magellan:Clay (MagIC), Blanco (OSIRIS)

REFERENCES

- Becker, W. & Aschenbach, B. 2002, in Proceedings of the 270. WE-Heraeus Seminar on Neutron Stars, Pulsars, and Supernova Remnants, ed. W. Becker, H. Lesch, & J. Trümper (Garching: MPE), 64, (astro-ph/0208466)
- Bergeron, P., Wesemael, F., & Beauchamp, A. 1995, *PASP*, 107, 1047
- Bignami, G. F., Caraveo, P. A., De Luca, A., & Mereghetti, S. 2003, *Nature*, 423, 725
- Bignami, G. F., Caraveo, P. A., & Mereghetti, S. 1992, *ApJ*, 389, L67
- Blackman, E. G. & Perna, R. 2004, *ApJ*, 601, L71
- Carter, L. M., Dickel, J. R., & Bomans, D. J. 1997, *PASP*, 109, 990
- Chakrabarty, D., Pivovarov, M. J., Hernquist, L. E., Heyl, J. S., & Narayan, R. 2001, *ApJ*, 548, 800
- Chatterjee, P., Hernquist, L., & Narayan, R. 2000, *ApJ*, 534, 373
- Chevalier, R. A. 1989, *ApJ*, 346, 847
- Cordes, J. M. & Shannon, R. M. 2006, Submitted to *ApJ*, (astro-ph/0605145)
- Cox, A. N. 2000, *Allen's Astrophysical Quantities*, 4th edn. (New York: AIP Press/Springer)
- De Luca, A., Mereghetti, S., Caraveo, P. A., Moroni, M., Mignani, R. P., & Bignami, G. F. 2004, *A&A*, 418, 625
- Depoy, D. L., Atwood, B., Byard, P. L., Frogel, J., & O'Brien, T. P. 1993, *Proc. SPIE*, 1946, 667
- Eikenberry, S. S., Fazio, G. G., Ransom, S. M., Middleditch, J., Kristian, J., & Pennypacker, C. R. 1997, *ApJ*, 477, 465
- Fan, X. 1999, *AJ*, 117, 2528
- Fazio, G. G. et al. 2004, *ApJS*, 154, 10
- Fesen, R. A., Pavlov, G. G., & Sanwal, D. 2006, *ApJ*, 636, 848
- Fryer, C. L., Colgate, S. A., & Pinto, P. A. 1999, *ApJ*, 511, 885
- Garmire, G. P., Pavlov, G. G., Garmire, A. B., & Zavlin, V. E. 2000, *IAU Circ.*, 7350, 2
- Giacani, E. B., Dubner, G. M., Green, A. J., Goss, W. M., & Gaensler, B. M. 2000, *AJ*, 119, 281
- Gotthelf, E. V., Halpern, J. P., & Seward, F. D. 2005, *ApJ*, 627, 390
- Gotthelf, E. V., Petre, R., & Vasisht, G. 1999, *ApJ*, 514, L107
- Helfand, D. J. & Becker, R. H. 1984, *Nature*, 307, 215
- Hui, C. Y. & Becker, W. 2005, *A&A*, submitted, (astro-ph/0508655)
- Indebetouw, R. et al. 2005, *ApJ*, 619, 931
- Kaplan, D. L., Kulkarni, S. R., & Murray, S. S. 2001, *ApJ*, 558, 270
- Kurucz, R. 1993, *ATLAS9 Stellar Atmosphere Programs and 2 km/s grid*. Kurucz CD-ROM No. 13. Cambridge, Mass.: Smithsonian Astrophysical Observatory, 1993., 13
- Landolt, A. U. 1992, *AJ*, 104, 340
- Lin, D. N. C., Woosley, S. E., & Bodenheimer, P. H. 1991, *Nature*, 353, 827
- Marsden, D., Lingenfelter, R. E., Rothschild, R. E., & Higdon, J. C. 2001, *ApJ*, 550, 397
- Martini, P., Persson, S. E., Murphy, D. C., Birk, C., Sheckman, S. A., Gunnels, S. M., & Koch, E. 2004, *Proc. SPIE*, 5492, 1653, (astro-ph/0406666)
- Matsui, Y., Long, K. S., & Tuohy, I. R. 1988, *ApJ*, 329, 838
- Michel, F. C. & Dessler, A. J. 1981, *ApJ*, 251, 654
- Monet, D. E. A. 1998, in *The PMM USNO-A2.0 Catalog* (U.S. Naval Observatory, Washington DC)
- Pavlov, G. G., Sanwal, D., Garmire, G. P., & Zavlin, V. E. 2002a, in *ASP Conf. Ser. 271: Neutron Stars in Supernova Remnants*, ed. P. O. Slane & B. M. Gaensler (San Francisco: ASP), 247, (astro-ph/0112322)
- Pavlov, G. G., Sanwal, D., & Teter, M. A. 2004, in *ASP Conf. Ser.: IAU Symposium 218: Young Neutron Stars and Their Environments*, ed. F. Camilo & B. M. Gaensler (San Francisco: ASP), 239, (astro-ph/0311526; PST04)
- Pavlov, G. G., Zavlin, V. E., Aschenbach, B., Trümper, J., & Sanwal, D. 2000, *ApJ*, 531, L53
- Pavlov, G. G., Zavlin, V. E., & Sanwal, D. 2002b, in Proceedings of the 270. WE-Heraeus Seminar on Neutron Stars, Pulsars, and Supernova Remnants, ed. W. Becker, H. Lesch, & J. Trümper (Garching: MPE), 273, (astro-ph/0206024)
- Pavlov, G. G., Zavlin, V. E., Sanwal, D., & Trümper, J. 2002c, *ApJ*, 569, L95
- Perna, R., Hernquist, L., & Narayan, R. 2000, *ApJ*, 541, 344
- Persson, S. E., Murphy, D. C., Krzeminski, W., Roth, M., & Rieke, M. J. 1998, *AJ*, 116, 2475
- Persson, S. E., West, S. C., Carr, D. M., Sivaramakrishnan, A., & Murphy, D. C. 1992, *PASP*, 104, 204
- Petre, R., Becker, C. M., & Winkler, P. F. 1996, *ApJ*, 465, L43
- Petre, R., Kriss, G. A., Winkler, P. F., & Canizares, C. R. 1982, *ApJ*, 258, 22
- Phinney, E. S. & Hansen, B. M. S. 1993, in *ASP Conf. Ser.: Planets around pulsars*, ed. J. A. Phillips, S. E. Thorsett, & S. R. Kulkarni, Vol. 36 (San Francisco: ASP), 371
- Podsiadlowski, P. 1993, in *ASP Conf. Ser.: Planets around pulsars*, ed. J. A. Phillips, S. E. Thorsett, & S. R. Kulkarni, Vol. 36 (San Francisco: ASP), 149
- Predehl, P. & Schmitt, J. H. M. M. 1995, *A&A*, 293, 889
- Reach, W. T. et al. 2006, *Infrared Array Camera Data Handbook*, ver. 3.0 (Pasadena: Spitzer Science Center)
- Reed, J. E., Hester, J. J., Fabian, A. C., & Winkler, P. F. 1995, *ApJ*, 440, 706
- Reynoso, E. M., Green, A. J., Johnston, S., Dubner, G. M., Giacani, E. B., & Goss, W. M. 2003, *MNRAS*, 345, 671
- Reynoso, E. M., Green, A. J., Johnston, S., Goss, W. M., Dubner, G. M., & Giacani, E. B. 2004, *Publications of the Astronomical Society of Australia*, 21, 82
- Rieke, G. H. & Lebofsky, M. J. 1985, *ApJ*, 288, 618
- Roger, R. S., Milne, D. K., Kesteven, M. J., Wellington, K. J., & Haynes, R. F. 1988, *ApJ*, 332, 940
- Sanwal, D., Pavlov, G. G., Zavlin, V. E., & Teter, M. A. 2002, *ApJ*, 574, L61
- Schlegel, D. J., Finkbeiner, D. P., & Davis, M. 1998, *ApJ*, 500, 525
- Sheckman, S. A. & Johns, M. 2003, *SPIE*, 4387, 910
- Skrutskie, M. F. et al. 2006, *AJ*, 131, 1163
- Smith, J. A. et al. 2002, *AJ*, 123, 2121
- Tananbaum, H. 1999, *IAU Circ.*, 7246, 1
- Thorstensen, J. R., Fesen, R. A., & van den Bergh, S. 2001, *AJ*, 122, 297
- Tuohy, I. & Garmire, G. 1980, *ApJ*, 239, L107
- Tuohy, I. R., Dopita, M. A., Garmire, G. P., & Manchester, R. N. 1983, *ApJ*, 268, 778
- Wang, Z. & Chakrabarty, D. 2002, in *ASP Conf. Ser. 271: Neutron Stars in Supernova Remnants*, ed. P. O. Slane & B. M. Gaensler (San Francisco: ASP), 271, (astro-ph/0112125)
- Wang, Z., Chakrabarty, D., & Kaplan, D. L. 2006, *Nature*, 440, 772
- Winkler, P. F., Tuttle, J. H., Kirshner, R. P., & Irwin, M. J. 1988, in *IAU Colloq. 101: Supernova Remnants and the Interstellar Medium*, ed. R. S. Roger & T. L. Landecker, 65
- Wolszczan, A. 1994, *Science*, 264, 538
- Wolszczan, A. & Frail, D. A. 1992, *Nature*, 355, 145
- Woods, P. M. & Thompson, C. 2004, in *Compact Stellar X-ray Sources*, ed. W. H. G. Lewin & M. van der Klis (Cambridge: Cambridge University Press), (astro-ph/0406133)
- Woosley, S. E. & Weaver, T. A. 1995, *ApJS*, 101, 181
- Zampieri, L., Colpi, M., Shapiro, S. L., & Wasserman, I. 1998, *ApJ*, 505, 876
- Zavlin, V. E. & Pavlov, G. G. 2004, *ApJ*, 616, 452
- Zavlin, V. E., Pavlov, G. G., & Sanwal, D. 2004, *ApJ*, 606, 444
- Zavlin, V. E., Pavlov, G. G., Sanwal, D., & Trümper, J. 2000, *ApJ*, 540, L25

TABLE 1
X-RAY PROPERTIES OF POINT SOURCES IN YOUNG SNRS

| Source | SNR | d (kpc) | Age (kyr) | $N_{\text{H}}/10^{22}$ (cm^{-2}) | $L_{\text{X}}^{\text{a}}/10^{33}$ (ergs s^{-1}) | Adopted Position(s) | Refs |
|-----------------------|-------------|--------------|--------------|--|---|---|-------|
| RX J0822.0–4300 | Pup A | 2.2 | 3.7 | 0.4 | 3.5 | 08 ^h 21 ^m 57 ^s .42 –43°00′16″.62 | 1–3 |
| 1E 1207.4–5209 | PKS 1209–52 | 2.1 | 7 | 0.13 | 2.4 | 12 ^h 10 ^m 00 ^s .92 –52°26′28″.35 ^c 12 ^h 10 ^m 00 ^s .88 –52°26′28″.66 | 2,4,5 |
| 1E 161348–5055.1 | RCW 103 | 3.3 | 1–3 | 1.7 | 1–60 ^b | 16 ^h 17 ^m 36 ^s .25 –51°02′24″.5 | 6–8 |
| CXOU J232327.8+584842 | Cas A | 3.4 | 0.32 | 1.3 | 2.0 | 23 ^h 23 ^m 27 ^s .94 +58°48′42″.51 | 9–12 |

REFERENCES. — (1) Petre et al. (1996); (2) Pavlov et al. (2004) (3) Hui & Becker (2005); (4) Helfand & Becker (1984); (5) De Luca et al. (2004); (6) Tuohy & Garmire (1980); (7) Pavlov et al. (2002a); (8) Becker & Aschenbach (2002); (9) Tananbaum (1999); (10) Pavlov et al. (2000); (11) Chakrabarty et al. (2001); (12) Fesen et al. (2006).

NOTE. — X-ray positions are all J2000.0, and have typical 90% uncertainties of 0′.6.

^aThe X-ray luminosity is in the range 0.5–10 keV for RX J0822.0–4300, 0.4–8 keV for 1E 1207.4–5209 and 1E 161348–5055.1, and 0.6–6 keV for CXOU J232327.8+584842.

^bThis source shows significant X-ray flux variations (Gotthelf et al. 1999).

^cThe two positions for this object are from *Chandra*/ACIS-S and *Chandra*/HRC-I, respectively; see § 3.2.

TABLE 2
SUMMARY OF OPTICAL/INFRARED OBSERVATIONS OF CCOs

| Object | Telescope | Instrument | Date | Band | Exposure (min) | Seeing (arcsec) | |
|-----------------------|----------------------|----------------------|-------------|-------------------|-------------------|--------------------|-------------------|
| RX J0822.0–4300 | Magellan Baade 6.5 m | MagIC | 2001-Mar-25 | r' | 10 | 0.7 | |
| | | | | i' | 10 | 0.6 | |
| | CTIO Blanco 4 m | OSIRIS | 2002-Feb-25 | J | 9 | 0.8 | |
| | | | | H | 18 | 0.8 | |
| | | | | K_s | 30 | 0.8 | |
| | | | | K_s | 30 | 0.6 | |
| | Magellan Baade 6.5 m | ClassicCam | 2002-Apr-09 | K_s | 30 | 0.6 | |
| | Magellan Clay 6.5 m | MagIC | 2003-Apr-05 | B | 30 | 0.7 | |
| | <i>Spitzer</i> | IRAC | 2004-Dec-18 | 4.5 μm | 77 | ... | |
| | | | | 8.0 μm | 75 | ... | |
| 1E 1207.4–5209 | Magellan Baade 6.5 m | MagIC | 2001-Mar-24 | r' | 9 | 0.9 | |
| | | | | i' | 10 | 1.0 | |
| | | | | g' | 10 | 1.0 | |
| | | | | u' | 5 | 1.0 | |
| | CTIO Blanco 4 m | OSIRIS | 2002-Feb-25 | J | 9 | 0.9 | |
| | | | | H | 18 | 0.9 | |
| | | | | K_s | 30 | 0.9 | |
| | | | | J | 15 | 0.5 | |
| | Magellan Baade 6.5 m | ClassicCam | 2002-Apr-08 | J | 15 | 0.5 | |
| | Magellan Baade 6.5 m | PANIC | 2004-Feb-12 | J | 30 | 0.5 | |
| | <i>Spitzer</i> | IRAC | 2005-Jul-17 | K_s | 40 | 0.5 | |
| | | | | 4.5 μm | 77 | ... | |
| | 1E 161348–5055.1 | Magellan Baade 6.5 m | ClassicCam | 2002-Apr-09 | 8.0 μm | 75 | ... |
| | | | | | J | 10 | 0.6 |
| H | | | | | 18 | 0.5 | |
| K_s | | | | | 15 | 0.5 | |
| Magellan Clay 6.5 m | | MagIC | 2003-Apr-05 | I | 50 | 0.7 | |
| | | | | <i>Spitzer</i> | IRAC | 2005-Mar-29 | 4.5 μm |
| <i>Spitzer</i> | | IRAC | 2005-Mar-29 | 8.0 μm | 75 | ... | |
| | | | | 4.5 μm | 77 | ... | |
| CXOU J232327.8+584842 | <i>Spitzer</i> | IRAC | 2004-Dec-15 | 4.5 μm | 77 | ... | |
| | | | | 8.0 μm | 75 | ... | |

TABLE 3
SKY BRIGHTNESSES (IN UNITS OF MJY/SR) AT THE POSITIONS OF CCOs

| Filter | RX J0822.0–4300 | 1E 1207.4–5209 | 1E 161348–5055.1 | CXOU J232327.8+584842 |
|-----------|-----------------|----------------|------------------|-----------------------|
| 4.5 μ | 0.10 | 0.03 | 3.14 | 0.70 |
| 8.0 μ | 4.21 | 1.49 | 11.75 | 81.8 |

TABLE 4
MAGNITUDES (DETECTED OR 3σ LIMITS) OF CCOs FROM OPTICAL/IR OBSERVATIONS

| Filter | Wavelength (Å) | RX J0822.0–4300 | 1E 1207.4–5209 | 1E 161348–5055.1 | CXOU J232327.8+584842 |
|----------------------|-------------------|-----------------|----------------|------------------|-----------------------|
| <i>u'</i> | 3540 | ... | >22.5 | ... | ... |
| <i>B</i> | 4400 | >26.5 | ... | ... | ... |
| <i>g'</i> | 4770 | ... | >23.9 | ... | ... |
| <i>r'</i> | 6230 | >25.0 | >24.3 | >24.8 | ... |
| <i>R</i> | 7000 | >26.0 | ... | ... | ... |
| <i>i'</i> | 7620 | >24.4 | >24.0 | >24.4 | ... |
| <i>I</i> | 9000 | ... | ... | >24.7 | ... |
| <i>J</i> | 12500 | >21.7 | >23.4 | >21.9 | ... |
| <i>H</i> | 16500 | >20.6 | >21.3 | 19.4±0.2 | ... |
| <i>K_s</i> | 21400 | >20.1 | >22.0 | 18.1±0.1 | ... |
| 4.5 μ^a | 44920 | >20.7 | >20.5 | >15.3 | >18.7 |
| 8.0 μ^a | 78700 | >17.7 | >17.6 | >13.5 | >14.6 |

^aThe zero magnitude flux are 179.7 Jy and 64.1 Jy for the 4.5 and 8.0 μm bands respectively (Reach et al. 2006).